© 2021. Published by The Company of Biologists Ltd | Development (2021) 148, dev196121. doi:10.1242/dev.196121

RESEARCH ARTICLE

Dynamics of *hunchback* translation in real-time and at single-mRNA resolution in the *Drosophila* embryo

Daisy J. Vinter, Caroline Hoppe, Thomas G. Minchington*, Catherine Sutcliffe and Hilary L. Ashe‡

ABSTRACT

The Hunchback (Hb) transcription factor is crucial for anterior-posterior patterning of the *Drosophila* embryo. The maternal *hb* mRNA acts as a paradigm for translational regulation due to its repression in the posterior of the embryo. However, little is known about the translatability of zygotically transcribed *hb* mRNAs. Here, we adapt the SunTag system, developed for imaging translation at single-mRNA resolution in tissue culture cells, to the *Drosophila* embryo to study the translation dynamics of zygotic *hb* mRNAs. Using single-molecule imaging in fixed and live embryos, we provide evidence for translational repression of zygotic *SunTag-hb* mRNAs. Whereas the proportion of *SunTag-hb* mRNAs translated is initially uniform, translation declines from the anterior over time until it becomes restricted to a posterior band in the expression domain. We discuss how regulated *hb* mRNA translation may help establish the sharp Hb expression boundary, which is a model for precision and noise during developmental patterning. Overall, our data show how use of the SunTag method on fixed and live embryos is a powerful combination for elucidating spatiotemporal regulation of mRNA translation in *Drosophila*.

KEY WORDS: Hunchback, *Drosophila* embryo, Translation, SunTag, Live imaging, MS2

INTRODUCTION

The gap gene *hunchback* (*hb*) is essential for body plan specification during *Drosophila* embryogenesis, primarily by establishing the gene expression boundaries of other gap genes through transcriptional repression (Hulskamp et al., 1990; Struhl et al., 1992). Embryos with complete loss of *hb* function lack gnathal and thoracic segments, show reversed polarity of the first two or three abdominal segments and fusion of the seventh and eighth abdominal segments (Lehmann and Nusslein-Volhard, 1987; Margolis et al., 1995). *hb* is maternally and zygotically expressed (Bender et al., 1988; Tautz et al., 1987). Maternally expressed *hb* mRNA is uniformly distributed in the embryo, but its translation is repressed in the posterior by Nanos, Pumilio, Brain Tumor and eIF4EHP (Cho et al., 2006; Hülskamp et al., 1989; Irish et al., 1989; Murata and Wharton, 1995; Sonoda and Wharton, 1999, 2001; Struhl, 1989; Wharton and Struhl, 1991).

Zygotic *hb* expression is dynamic, with spatial and temporal regulation relying on two promoters and three enhancers. Initially *hb* is transcribed from the proximal P2 promoter (Margolis et al., 1995; Schröder et al., 1988) in a broad anterior domain in nuclear cycle (nc) 11 embryos (Bender et al., 1988; Tautz et al., 1987; Tautz and Pfeifle, 1989), in response to the Bicoid (Bcd) gradient (Driever and Nüsslein-Volhard, 1989; Struhl et al., 1989). This expression in the anterior half of the embryo persists into early nc14, when *hb* mRNAs from the P2 promoter also appear transiently in a posterior cap. From mid-nc14, both the P1 and P2 promoters are active, with the resulting transcripts accumulating in a stripe positioned at the posterior boundary of the anterior domain of *hb* expression, around 50% of the egg length (EL), as well as in the posterior region of the embryo (Margolis et al., 1995). By this time, the broad anterior domain of *hb* mRNA has decayed so that only two weaker stripes of mRNA are detectable in the anterior, in addition to the newly activated central stripe (Margolis et al., 1995; Tautz and Pfeifle, 1989). Early *hb* expression in the anterior half of the embryo is controlled by Bcd-responsive proximal and shadow enhancers (Driever and Nüsslein-Volhard, 1989; Margolis et al., 1995; Perry et al., 2011; Struhl et al., 1989), whereas a stripe enhancer activates transcription in both the central and posterior stripes (Margolis et al., 1995; Perry et al., 2012). The stripe enhancer is ubiquitously activated, but two stripes are formed because of the action of repressors encoded by other gap genes (Perry et al., 2012).

Hb protein distribution mirrors that of the zygotic mRNA pattern described earlier, except that the protein persists in the entire anterior half of mid-late nc14 embryos, likely because of slower degradation of the protein than of mRNA (Perry et al., 2012; Tautz and Pfeifle, 1989; Wu et al., 2001). The anterior Hb domain has a steep boundary of Hb protein in the centre of the embryo, in part because of expression from the stripe enhancer (Perry et al., 2012). Overall, much is known about the transcriptional regulation of *hb*, including quantitative live-imaging studies of the output from the proximal enhancer and P2 promoter, with nascent transcription detected as early as nc9-10 (Garcia et al., 2013; Lucas et al., 2013). In comparison, little is known about the translatability of zygotic *hb* mRNAs in space and time during early embryogenesis.

The *Drosophila* embryo represents a paradigm for understanding how translational control can underpin developmental patterning, e.g. through studies of the translational repression of the *oskar*, *caudal* and maternal *hb* mRNAs (Lasko, 2012). In addition, ribosome profiling has provided new insights into the control of translation of the entire transcriptome in *Drosophila* embryos (Dunn et al., 2013; Eichhorn et al., 2016). However, the temporal dynamics of mRNA translation have been less well studied because of the absence of a method to image and quantitate translation at a single-mRNA level in *Drosophila*. Recently, the SunTag method has been

Faculty of Biology, Medicine and Health, University of Manchester, Manchester M13 9PT, UK.
*Present address: Institute of Science and Technology Austria (IST Austria), Am Campus 1, 3400 Klosterneuburg, Austria.

‡Author for correspondence (hilary.ashe@manchester.ac.uk)

D.J.V., 0000-0002-0414-762X; C.H., 0000-0001-5600-309X; T.G.M., 0000-0002-7501-4760; C.S., 0000-0003-0309-0278; H.L.A., 0000-0002-8379-7830

Handling Editor: Thomas Lecuit
Received 18 August 2020; Accepted 10 March 2021

Development (2021) 148, dev196121. doi:10.1242/dev.196121

developed in tissue culture cells, in which 24 copies of a GCN4 peptide, the SunTag, is introduced at the start of the coding sequence. This SunTag array can be detected as it emerges from the ribosome exit channel, by the binding of a co-expressed single-chain variable fragment antibody (scFv) fused to GFP (Pichon et al., 2016; Tanenbaum et al., 2014; Wang et al., 2016; Wu et al., 2016; Yan et al., 2016). In combination with the MS2 system to visualise individual mRNAs, translation can be followed in real-time and quantitated. As a result, this method has provided powerful new insights into the regulation of translation; e.g. localisation or isoform-dependent differences in translation efficiency (Voigt et al., 2017; Wu et al., 2016; Yan et al., 2016).

By adapting the SunTag system for *Drosophila* embryos, we have studied the translation dynamics of zygotic *hb* mRNAs in both fixed and live embryos, which reveals temporal regulation of *hb* mRNA translation in the early embryo. Translation is uniform across the *hb* expression domain in nc12-13, but then becomes repressed in the anterior so that *hb* mRNA translation persists in only a band of cells at the posterior of the expression domain in nc14. These results suggest a previously unknown translational regulation of zygotic *hb* mRNAs, which may contribute to the refinement and precision of the Hb protein boundary, impacting downstream developmental patterning.

RESULTS

In order to visualise translation of single mRNAs in the early *Drosophila* embryo, we focused on the gap gene *hb* and adapted the SunTag method, which has previously been used to monitor translation of mRNAs in tissue culture cells and cultured neurons (Pichon et al., 2016; Wang et al., 2016; Wu et al., 2016; Yan et al., 2016). We generated a *SunTag-hb* reporter gene, under the control of the P2 promoter and primary Bicoid-responsive enhancer (Driever and Nüsslein-Volhard, 1989; Struhl et al., 1989), which carries an array of 24 copies of the SunTag peptide at its N terminus (Fig. 1A). This peptide is recognised by scFv fused to mNeonGreen (NG), which is expressed as a second transgene, under the control of the *nanos* (*nos*) promoter to allow maternal expression (Fig. 1A). We added a nuclear localisation signal to the scFv-NG protein to reduce cytoplasmic accumulation of unbound scFv-NG, as described previously (Pichon et al., 2016), to improve the signal-to-noise ratio in the cytoplasm and facilitate detection of translation of individual mRNAs. As a result, NG antibody staining of embryos carrying only the scFv-NG transgene shows uniform nuclear NG signals throughout the embryo during early stages of development (Fig. 1B).

First, we studied fixed embryos maternally expressing *scFv-NG* and carrying a single copy of the *SunTag-hb* transgene. We used smFISH probes against the SunTag sequences to visualise *SunTag-hb* mRNAs, combined with NG antibody staining to detect the scFv-NG protein (Fig. 1A). Visualisation of *SunTag-hb* mRNAs in a nc13 embryo reveals their localisation in a broad anterior domain, with bright transcription foci and the dimmer signals associated with single mRNAs (Fig. 1C). It is also clear from the scFv-NG staining that, although this protein is predominantly nuclear in the posterior region of the embryo, as expected because of the presence of the nuclear localisation signal (NLS), a cytoplasmic NG signal is observed in the anterior (Fig. 1C, compare with Fig. 1Bii). A higher magnification image from the anterior region of a nc13 embryo allows individual mRNAs to be visualised (Fig. 1D, pink arrowheads). A subset of these mRNAs has a colocalising NG signal (Fig. 1D, white arrowheads), consistent with these mRNAs being translated. In addition, weaker green puncta are detected that are not colocalised with a mRNA signal, which are likely single proteins within the cytoplasm (Fig. 1D, green arrowheads).

As we can detect translation of single mRNAs, we determined the *hb* mRNA translation efficiency depending on position in the expression domain. First, we quantitated the total number of *SunTag-hb* mRNAs in early nc12 (Fig. 2A). Given that the embryo is not cellularised at this stage, we assigned mRNAs to the nearest nucleus, giving us the mRNA number per nuclear territory. To focus only on cytoplasmic mRNAs and proteins, we masked nuclei to exclude signals in the nucleus from our quantitation (see Materials and Methods for more details). The cytoplasmic *SunTag-hb* mRNA number, plotted as the mean from three embryos, shows a graded distribution with an increase toward the central region of the *hb* expression domain, followed by a decrease in the posterior half (Fig. 2Bi). This mRNA profile is similar to that described for the mRNA output from the primary *hb* enhancer (Garcia et al., 2013) and for endogenous *hb* mRNAs at nc12 (Little et al., 2013). Quantitation of the number of *SunTag-hb* mRNAs being translated shows a similar graded profile to that of the total mRNA (Fig. 2Bii). Consistent with this, the proportion of *SunTag-hb* mRNAs being translated is constant at ∼55% regardless of position within the expression domain (Fig. 2Biii). The mean number of cytoplasmic *SunTag-hb* mRNAs, with the number and proportion translated for each embryo, is shown in Fig. S1A; all the data points for a representative embryo are shown in Fig. S1B.

To investigate translation of *SunTag-hb* mRNAs through development, we repeated this imaging and quantitation for nc13 embryos (Fig. 2C; the representative heatmap shown is for the embryo image in Fig. 1D). At this stage, the mRNA distribution is similar to that in nc12, although mRNA number has increased (Fig. 2Ci). The numbers of translated mRNAs are also increased and again their distribution mirrors that of the total mRNA profile (Fig. 2Cii), so that the percentage translated is uniform (∼50%) across the expression domain (Fig. 2Ciii). The mean numbers of total and translated *SunTag-hb* mRNAs are shown for individual nc13 embryos in Fig. S1C, in addition to the data for each nuclear territory for a representative embryo (Fig. S1D).

Next, we focussed on early nc14 embryos, recognised by the presence of *SunTag-hb* transcription sites, because the proximal enhancer activates *hb* transcription only early in nc14 (Garcia et al., 2013). Visualisation of *SunTag-hb* mRNAs and NG signal in early nc14 embryos reveals a different distribution of translation sites, with the highest NG signal detected in a posterior band within the expression domain (Fig. 3A). The higher magnification images show the paucity of translation sites in the anterior, despite high mRNA density compared with the posterior (Fig. 3A). Quantitation of the total number of cytoplasmic *SunTag-hb* mRNAs per nuclear territory in early nc14 (Fig. 3Bi, Fig. S1Ei,Fi) reveals a similar profile to that observed in nc13, with an increase in the total mRNA number, again consistent with published data for the output from the *hb* primary enhancer (Bothma et al., 2015; Garcia et al., 2013) and endogenous *hb* at this stage (Little et al., 2013). However, at this stage, the profile of *SunTag-hb* translated mRNAs differs from the mRNA distribution and instead peaks at the posterior of the expression domain (Fig. 3Bii, Fig. S1Eii,Fii). As such, the proportion of mRNAs translated is <10% in the anterior of the expression domain, increasing to ∼60% in the posterior (Fig. 3Biii, Fig. S1Eiii). These data suggest that there is an active translation repression mechanism in the anterior at nc14, but not in the posterior of the expression domain, where translation of *SunTag-hb* mRNAs persists.

However, an alternative explanation of these data could be that the scFv-NG is limiting and has become depleted in the anterior region of the *SunTag-hb* expression domain, where the mRNA

Development (2021) 148, dev196121. doi:10.1242/dev.196121

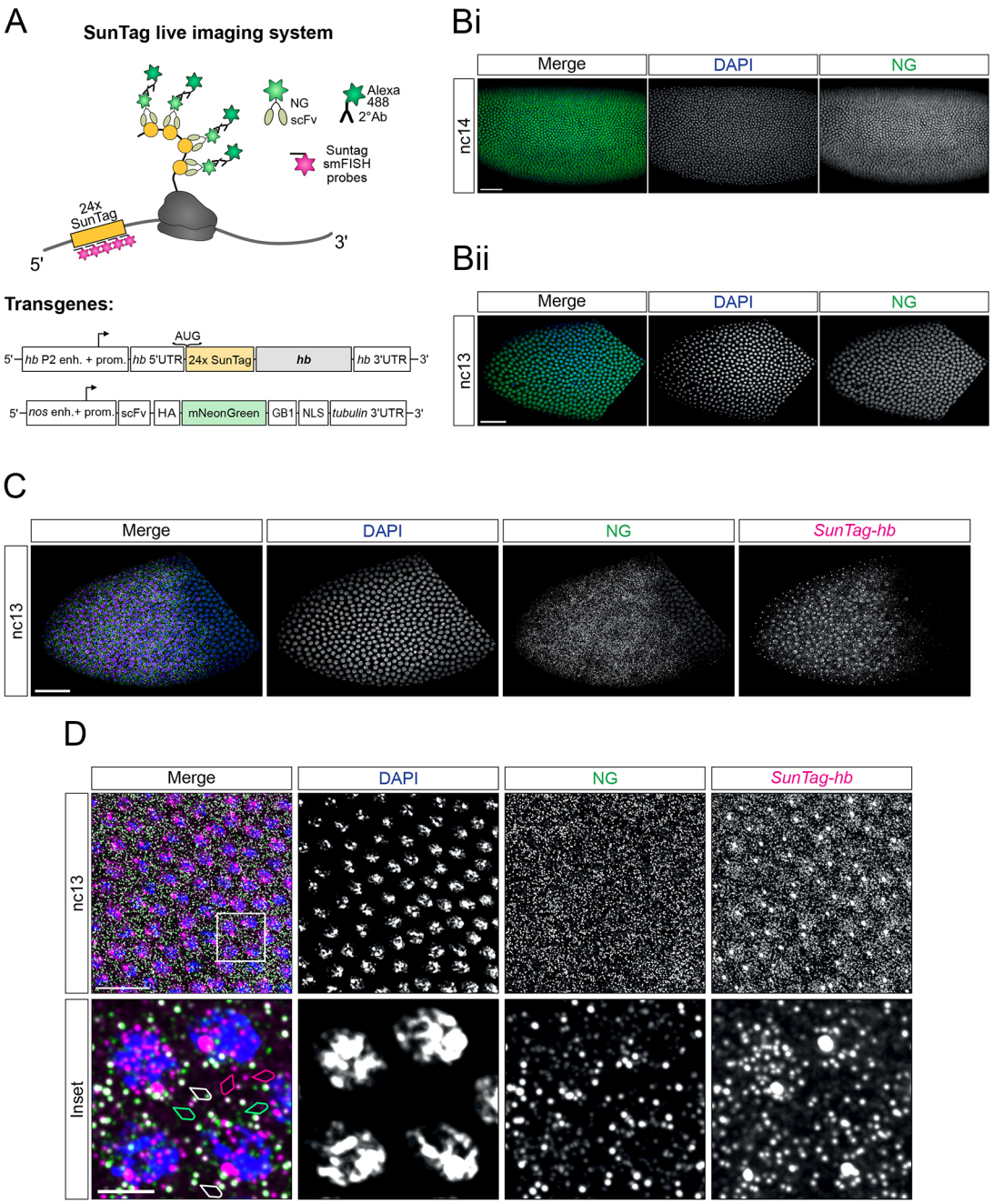

Fig. 1. Visualisation of translation of single *SunTag-hb* mRNAs in the *Drosophila* embryo. (A) Schematic showing translation of the *SunTag-hb* mRNA. SunTag peptides are recognised by a scFv-NG fusion protein that is detected by an antibody stain. mRNAs are recognised by smFISH probes against the SunTag sequence. Schematics show the organisation of the transgenes used for visualisation of translation. (B) (i) *Drosophila* nc14 embryo from a female maternally expressing *scFv-NG* crossed to a wild-type male, stained with DAPI (blue) and anti-NG (green). (ii) As in Bi, except the anterior of a nc13 embryo is shown. (C) Anterior region of a nc13 embryo from a female maternally expressing *scFv-NG* crossed to a male carrying the *SunTag-hb* transgene, stained with DAPI (blue), anti-NG (green) and *SunTag* smFISH probes (magenta). (D) As in C but higher magnification views are shown. The bottom panel shows a maximum projection of nine slices for the boxed region of interest. White arrows show colocalised scFv-NG and *SunTag-hb* smFISH signals representing translated mRNAs. Magenta arrows identify *SunTag-hb* smFISH signals that are not colocalised, which are untranslated mRNAs. Green arrows show weaker scFv-NG signals that are not colocalised, which are likely single proteins. Scale bars: 50 µm in B and C, 20 µm in D (top panel); 5 µm in D (lower panel).

number is highest in nc12-14. Therefore, we addressed this in two ways. First, we introduced one and two extra copies of the maternally expressed scFv-NG fusion protein into embryos and visualised *SunTag-hb* mRNA translation at nc14. These extra copies increase the scFv-NG protein concentration in the early embryo (Fig. S2A,B). Embryos with three or four copies of the scFv-NG fusion protein still show higher translation in the posterior of the expression domain than in the anterior at nc14 (Fig. S2C,D). Second, to increase the amount of scFv-NG protein available in the cytoplasm to bind the SunTag peptides, we removed the NLS we had added to the scFv-NG fusion protein. In the presence of maternally expressed scFv-NG (no NLS), the band of translation sites is again observed at nc14 (Fig. S2E). Together, these controls suggest that the very low proportion of *SunTag-hb* mRNAs

Development (2021) 148, dev196121. doi:10.1242/dev.196121

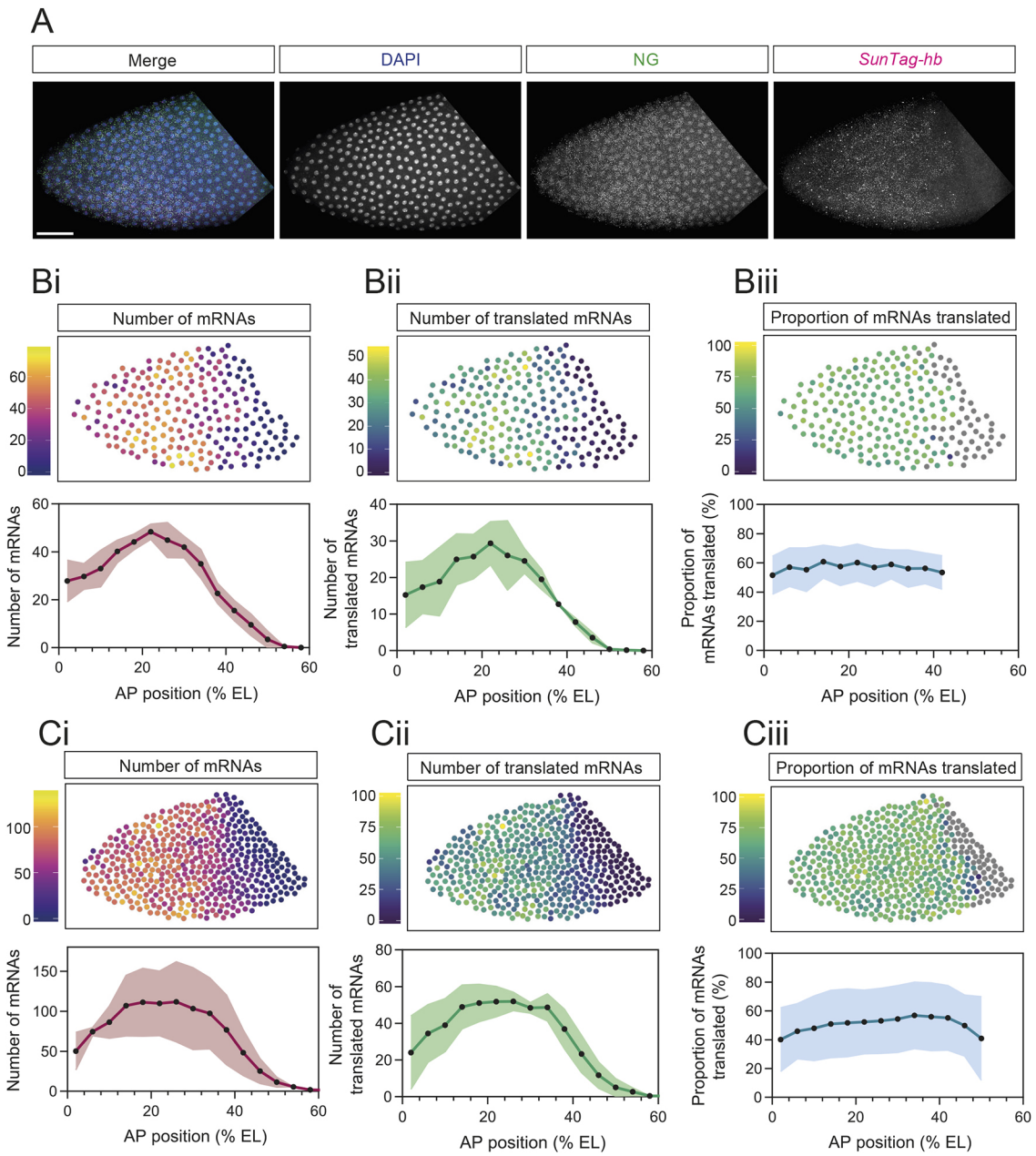

Fig. 2. Uniform translation of *SunTag-hb* mRNAs across the expression domain in nc12 and 13. (A) Anterior region of a fixed *Drosophila* nc12 embryo with maternal and zygotic expression of the *scFv-NG* and *SunTag-hb* transgenes, respectively, stained with DAPI (blue), anti-NG (green) and *SunTag* smFISH probes (magenta). (B) Quantitation per nuclear territory of total cytoplasmic mRNAs (i), translated mRNAs (ii), and percentage of mRNAs translated (iii) in nc12 embryos. Heat maps correspond to the embryo image in A. % EL is estimated based on an embryo length of 500 µm. Nuclear territories are binned along the AP axis (bin size 20 µm) and mean values per bin are reported. Data are shown as mean±s.d., *n*=3 embryos. (C) As in B, except the quantitation is for nc13 embryos and the heatmaps are for the embryo shown in Fig. 1D. Scale bar: 50 µm in A.

translated in the anterior in nc14 embryos is not due to limiting scFv-NG protein, but instead reflects a repression mechanism that restricts *SunTag-hb* mRNA translation to a posterior band positioned ∼30-50% EL.

We also used our ability to visualise translation of *SunTag-hb* mRNAs at single-mRNA resolution to address their compaction, because recent studies on a subset of mRNAs in mammalian cells found that they shift to a more open conformation when they are being translated (Adivarahan et al., 2018; Khong and Parker, 2018). We assessed the compaction of *SunTag-hb* mRNAs during translation by using smFISH probes against the *SunTag* sequences and smiFISH probes against *hb* sequences, positioned at the 5′ and 3′ ends of the mRNA, respectively (Fig. 4A). A representative nc14 embryo image is shown in Fig. 4Bi, with two regions of interest captured at higher magnification shown in Fig. 4Bii. Using the images captured at higher magnification, we classified mRNAs as being translated or not based on the presence or absence of a colocalised NG signal, and measured the distance between the probes following 3D rendering of the signals (Fig. 4Biii, see also Materials and Methods). This analysis reveals a range of distances between the 5′ and 3′ ends of translated and untranslated mRNAs (Fig. 4Ci shows the spread of data for a

Development (2021) 148, dev196121. doi:10.1242/dev.196121

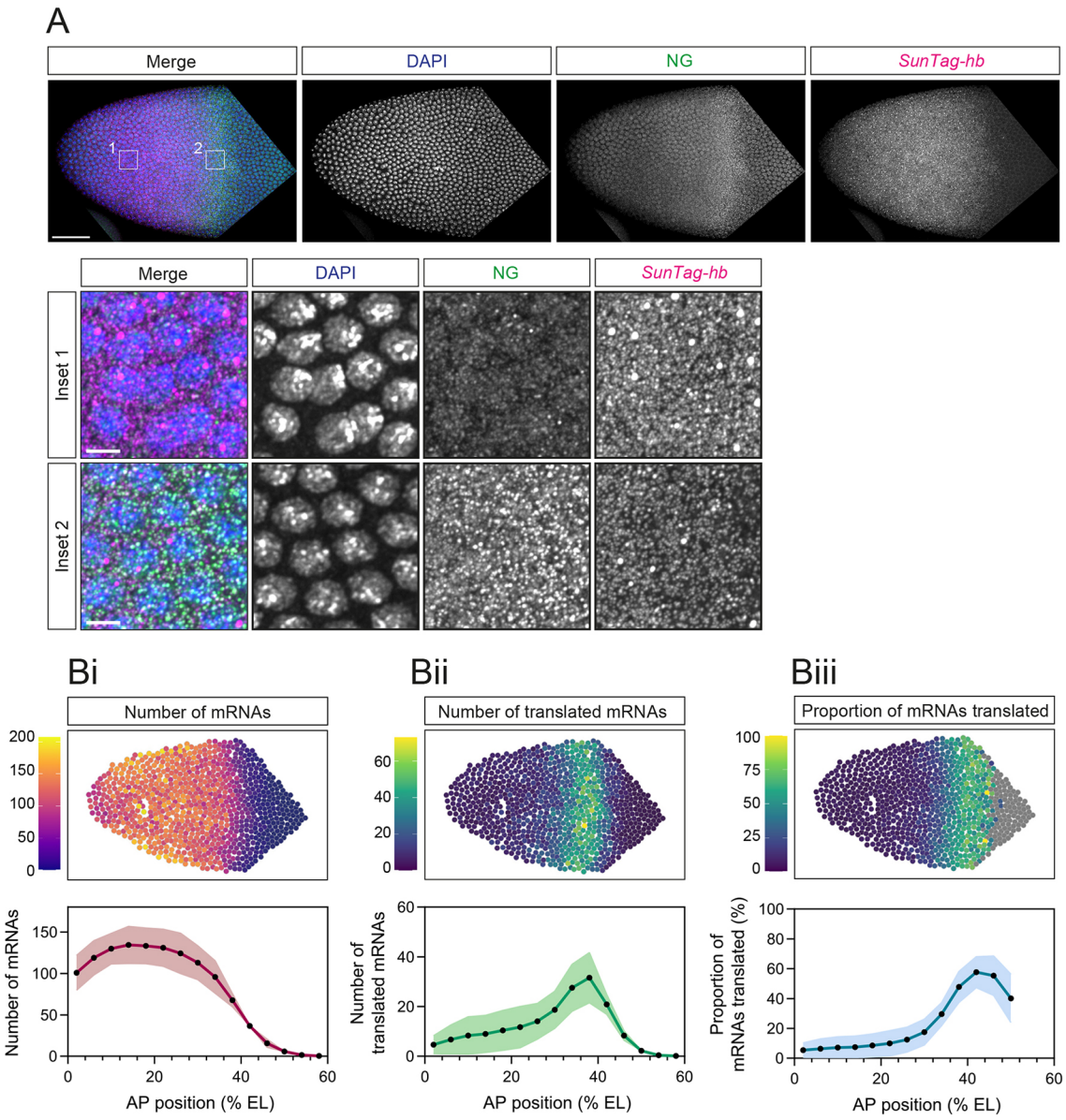

Fig. 3. Translation of *SunTag-hb* mRNAs occurs in a band in nc14. (A) Anterior region of a fixed nc14 *Drosophila scFv-NG*, *SunTag-hb* embryo stained with DAPI (blue), anti-NG (green) and *SunTag* smFISH probes (magenta). Inset regions from anterior (1) and posterior (2) regions of the expression domain. (B) Quantitation of total cytoplasmic mRNAs (i), translated mRNAs (ii) and percentage of mRNAs translated (Biii) per nuclear territory. Heat maps correspond to the embryo image in A. % EL is estimated based on an embryo length of 500 µm. Nuclear territories are binned along the AP axis (bin size 20 µm) and mean values per bin are determined. Data are shown as mean±s.d., *n*=3 embryos. Scale bars: 50 µm in A; 5 µm in A insets.

representative nc14 embryo). The median distance is significantly higher for translating mRNAs compared with those that are not, at both nc13 and nc14 (Fig. 4Cii). These data are consistent with the *SunTag-hb* mRNAs being in a slightly more open conformation during translation elongation. However, we note that the SunTag system lacks the resolution to visualise mRNAs specifically at the translation initiation step, because elongation of the ribosome through the SunTag peptides is necessary in order to classify the mRNA as being translated.

We also used these images to estimate the number of ribosomes translating *SunTag-hb* mRNAs, based on the relative intensity of the NG signal for translation sites versus single proteins (Fig. 4D). Additionally, we applied a correction to account for the signal on the mRNA potentially arising from only partial translation of the SunTag sequence (Pichon et al., 2016) (see Materials and Methods for details). Given that we detect a low proportion of relatively strong NG signals that are not colocalised with mRNAs (Fig. S5D), which likely reflect scFv-NG aggregates, to classify translation sites we only quantitated NG signals that colocalised with a *SunTag-hb* mRNA signal (see Materials and Methods). We detect a range in the number of translating ribosomes on *SunTag-hb* mRNAs (Fig. 4Di), with a mean of ∼20 ribosomes/mRNA in both the anterior and posterior of a nc13 embryo (Fig. 4Dii). In nc14 embryos, the *SunTag-hb* mRNAs are less heavily translated (Fig. 4D). Moreover, there is a spatial difference in ribosome density, with a significantly lower number of ribosomes translating *SunTag-hb* mRNAs in the anterior than in the posterior in nc14. Our data from nc13 and nc14 embryos suggest inter-ribosomal distances of between 180 and 690 nucleotides (nt) on *SunTag-hb* mRNAs, which is similar to the 160-910 nt range of inter-

Development (2021) 148, dev196121. doi:10.1242/dev.196121

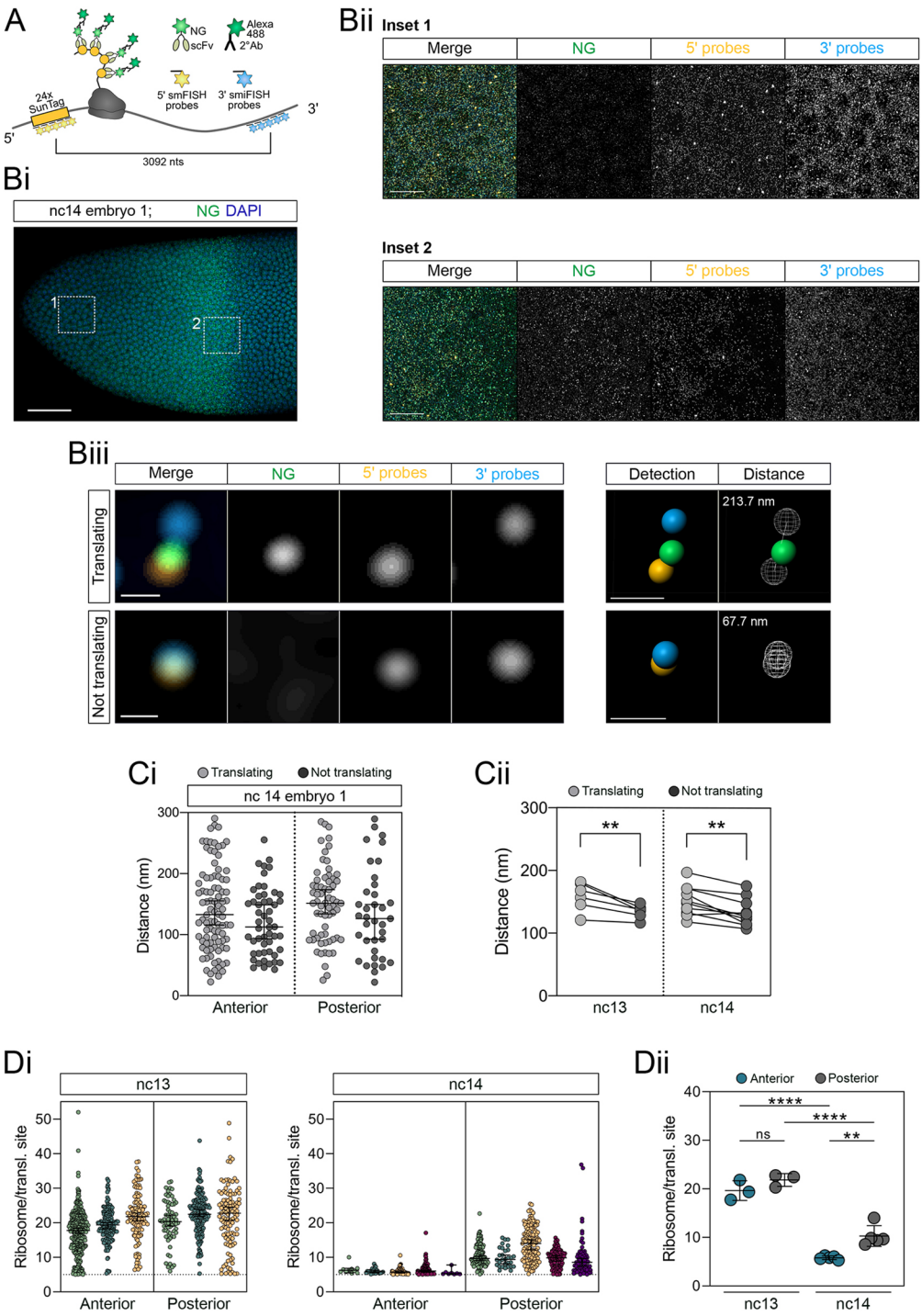

Fig. 4. Compaction of *SunTag-hb* mRNAs and ribosome density within the expression domain. (A) Schematic showing *SunTag-hb* mRNA translation, SunTag peptides are recognised by the scFv-NG fusion protein and visualised by antibody staining. The 5′ *SunTag* sequences are recognised by smFISH probes and the 3′UTR region by smiFISH probes; the centres of each probe set are separated by 3092 nts. (Bi) Anterior region of a fixed *scFv-NG; SunTag-hb* nc14 embryo showing DAPI (blue) and anti-NG (green) staining; the mRNA signals are not shown. (Bii) Enlarged regions from Bi showing an anterior (1) and posterior (2) view of the *hb* expression domain stained with *SunTag* 5′ (orange) and *hb* 3′ (cyan) probes, and anti-NG (green). Here, 15 optical slices are maximum intensity projected; the *hb* 3′ probes also detect endogenous *hb* mRNAs. (Biii) Enlarged view of individual *hb* mRNA molecules. Translating mRNAs were identified by colocalisation of the 5′ probe signal with NG. Fluorescent signals were identified using Imaris software (Detection panel) and the closest distance between the 5′ and 3′ probe signal was computed in 3D (Distance panel). (Ci,Cii) Quantitation of mRNA compaction, reported as (Ci) distances between the 5′ and 3′ probe sets for translating (light grey) and non-translating (dark grey) mRNAs in the inset regions shown in Bii and Cii as the median of biological replicates. The lines connect the data from each biological replicate. n=52, 92, 37 and 64 mRNA molecules (Ci) and n=5 (nc13) and 7 (nc14) embryos (Cii). $^{**}P$<0.01; data are shown as median±95% confidence intervals (Ci) and paired Student's t-test (Cii). (Di) Quantitation of ribosome numbers present in translation sites in the anterior and posterior regions of nc13 and nc14 embryos. (Dii) Comparison of the average ribosome numbers between biological replicates. Ribosome numbers greater than five were detected in this analysis (see Materials and Methods for details). $^{**}P$<0.01, $^{****}P$<0.0001; ns, not significant; data are shown as median±95% confidence intervals (Di) and as mean±s.d. (Dii). n=345, 146, 114, 65, 160 and 113 translation sites (nc13), and 10, 22, 68, 99, 8, 123, 30, 138, 97 and 67 translation sites (nc14) (Di). n=3 (nc13) and 5 (nc14) embryos (Dii). A one-way ANOVA with a Tukey's multiple comparisons test was used in Dii.

Development (2021) 148, dev196121. doi:10.1242/dev.196121

ribosomal distances reported in mammalian cells (Morisaki and Stasevich, 2018). Together, the data presented above and our quantitation of ribosome number suggest that, in nc14 embryos, the number of mRNAs being translated in the anterior is low and their translation efficiency is poor.

We next used the SunTag system to image translation in living embryos. First, we imaged embryos that carried the *SunTag-hb* and *scFv-NG* transgenes to visualise translation sites (Fig. 5A), in addition to Histone(His)-RFP to label the nuclei for precise ageing of the embryos. We imaged a narrow field of view in the anterior of the embryo to balance optimal temporal and spatial resolution (Movie 1, Fig. 5Bi). In this live imaging, we detect a lower number of translation sites than in the fixed images, because we are only detecting the brightest translation sites. Imaging at higher magnification and with increased laser power will improve sensitivity, but the advantage of our approach here is that imaging the area extending across one-third of the anterior-posterior (AP) axis will provide us with an overview of the global translation dynamics. Indeed, analysis of this movie reveals how the band of translation sites in the centre of the embryo evolves during development.

The dynamic distribution of translation sites through developmental time is shown in stills from Movie 1, by focussing on a region in the anterior and posterior (Fig. 5Bii). These data show that, initially in nc11, translation sites are clearly visible in the anterior but not posterior region of the expression domain (Fig. 5Bii). In nc12, translation sites are detected in both regions,

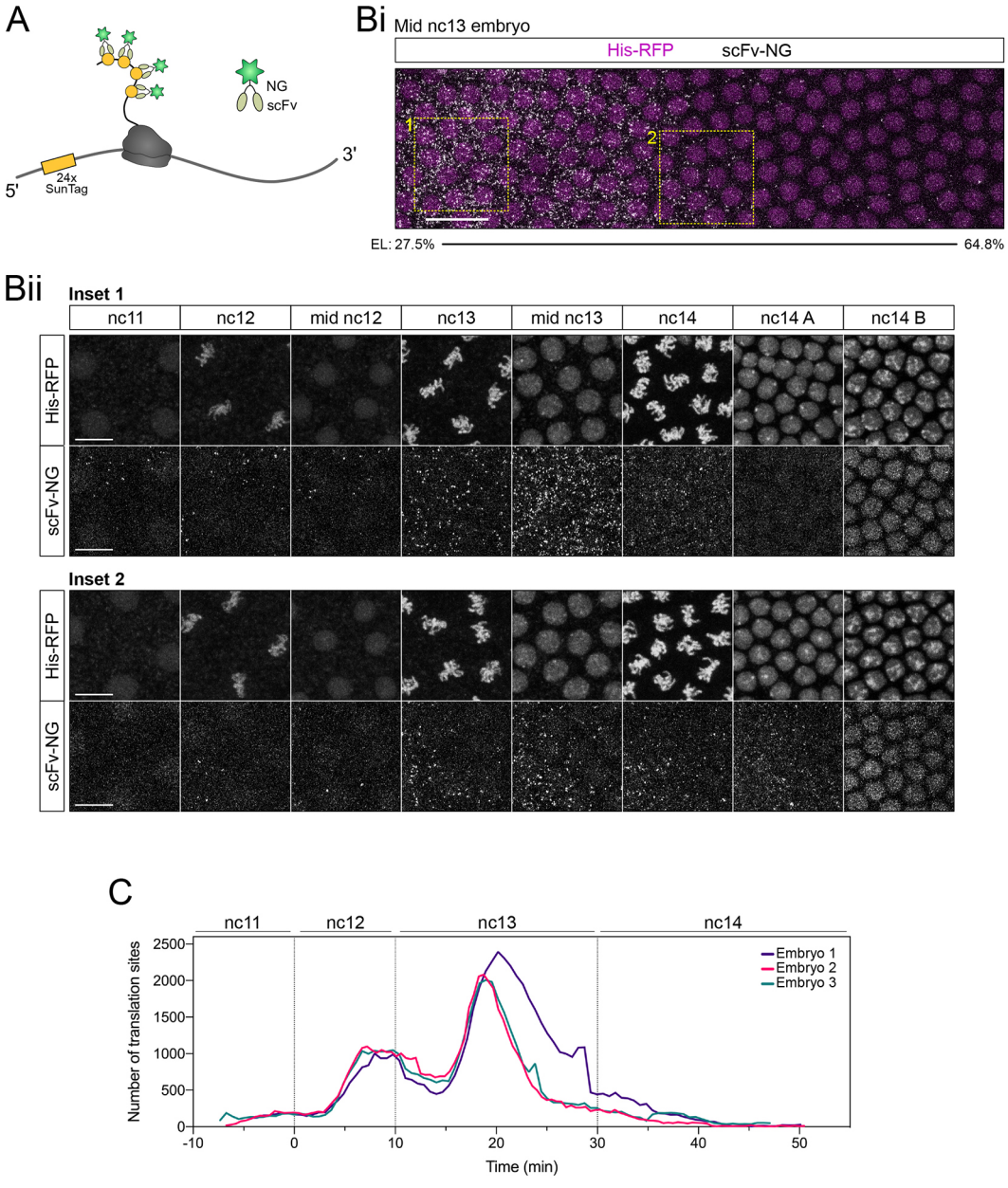

Fig. 5. Live imaging using the SunTag system reveals global translation dynamics of *SunTag-hb* mRNAs. (A) Schematic of a *SunTag-hb* mRNA being translated and recognised by scFv-NG. (B) (Bi) Maximum projected still from Movie 1 at mid nc13 showing *hb* translation by scFv-NG fluorescence (grey) and nuclei labelled with His-RFP (magenta). (Bii) Enlarged regions from Bi showing an anterior (1) and posterior (2) view of *SunTag-hb* translation through developmental time. (C) Quantitation of translation site number over developmental time. Time-lapse data sets were aligned with t=0 min at the onset of nc12, *n*=3 biological replicates. Scale bars: 20 µm in Bi; 10 µm in Bii.

Development (2021) 148, dev196121. doi:10.1242/dev.196121

although there are fewer in the posterior (Fig. 5Bii). In nc13, there is a large increase in the number of translation sites, again with more in the anterior, consistent with the data from fixed embryos (Fig. 2). This peak in *SunTag-hb* mRNA translation during nc13 is also obvious when the total number of translation sites is quantitated over time for three biological repeats (Fig. 5C, Fig. S3B). In nc14 embryos, translation sites are initially detected in both the anterior and posterior; however, over time, translation sites are only detected in the posterior (Fig. 5Bii), consistent with our analysis of fixed embryos (Fig. 3). Later in nc14, no translation sites are detected and instead the intensity of the nuclear SunTag-Hb signal increases, consistent with nuclear import (Fig. 5Bii).

We also used the live-imaging data to plot the profiles of translation sites in bins along the AP axis over time in nc12-14 for each of the biological repeats (Fig. S3A). Initially in nc12, the translation site profile is broadly similar to the mRNA distribution, with declining numbers in the posterior (Fig. S3A). The number of translation sites increases throughout nc12 and during the first ∼10 min of nc13, after which the number starts to decline. Towards the end of nc13 for embryos 2 and 3, or start of nc14 for embryo 1, the translation site profiles change shape so that the position on the AP axis with the highest number of translation site moves progressively posteriorly (Fig. S3A). There is some variation in the time at which this happens, consistent with biological variation. Nonetheless, these live-imaging data show that the domain of translation contracts from the anterior over time, leaving only a band of translating *SunTag-hb* mRNAs in the embryo at ∼35-55% EL early in nc14, consistent with our data from fixed embryos (Fig. 3).

In order to visualise *SunTag-hb* mRNAs and translation sites in living embryos, we inserted a cassette carrying 128 copies of the MS2 loops, which allows high sensitivity of detection (Tantale et al., 2016), into the 3′-untranslated region (UTR) of the *SunTag-hb* transgene (Fig. 6A). *SunTag* smFISH and NG antibody staining of fixed embryos carrying this transgene show that insertion of the 128x MS2 cassette does not alter the mRNA translation profile (Fig. S4). Live imaging of this *SunTag-hb-MS2* transgene in embryos that also maternally express MCP-RFP (Halstead et al., 2016) and scFv-NG allows visualisation of the transcription site in each nucleus (Fig. 6Bi). However, the density of mRNAs in the cytoplasm and their speed of movement prevents the detection and tracking of individual mRNAs in subsequent frames (Fig. 6Bii, Movie 2).

To facilitate longer term tracking of individual mRNAs, we used an approach described for the SunTag method in tissue culture cells, which is to add a membrane-targeting CAAX sequence to MCP (Yan et al., 2016). We also expressed MCP as a tandem dimer to promote full occupancy of the MS2 stem loops and fused two copies of mRuby3 to MCP to avoid an associated loss of fluorescence because of MCP binding the loops as a dimer (Wu et al., 2012) (Fig. 6C). Given that the early *Drosophila* embryo is not cellularised, the tdMCP-mRuby3-CAAX fusion protein is concentrated on the available apical membrane. Consistent with this, the membrane localisation of the tdMCP-mRuby3-CAAX protein allows membrane ingression to be followed in nc14 (Fig. 6D). Imaging the *SunTag-hb-MS2* transgene in embryos maternally expressing the *tdMCP-mRuby3-CAAX* transgene allows visualisation of translation sites (Movie 3). Note that the embryo in Movie 3 was imaged in a single plane to allow faster temporal resolution. Stills from Movie 3 show translation sites, which are largely immobile owing to the membrane tethering and can be tracked over time (Fig. 6E, white arrowheads). In addition, single proteins are visible that are highly mobile and move in and out of the imaged plane in successive frames (Fig. 6E, orange arrowheads). We also detect some bright NG puncta that do not colocalise with mRNAs (Fig. S5C), as described earlier for the fixed images. This mRNA tethering approach allows the tracking of translation sites in living embryos for >5 min; the NG fluorescence intensity traces of two *SunTag-hb-MS2* mRNAs in Movie 3 are shown in Fig. S5A.

This longer term imaging of *SunTag-hb-MS2* mRNA translation sites also allows different events in the translation cycle to be visualised. For example, we observed the release of a newly synthesised SunTag-Hb protein (Fig. 6F, orange arrowhead) from the translation site (Fig. 6F, blue arrowhead, see also Movie 4). Consistent with this, the sum of the NG fluorescence intensities of the mature released protein and its translation site is equivalent to that of the translation site in the preceding frame (Fig. 6F). This quantitation also suggests that, when the protein is released, there are three or four ribosomes translating the mRNA in the translation site. In addition, we have been able to visualise termination of *SunTag-hb-MS2* mRNA translation (Movie 5, Fig. 6G). When the mature protein (Fig. 6G, orange arrowhead) is released from the translation site (Fig. 6G, white arrowhead), a bright mRuby3 fluorescent signal is visible (Fig. 6G, yellow arrowhead), consistent with further clustering of tdMCP-mRuby3-CAAX proteins when they are bound to the *SunTag-hb-MS2* mRNA. Finally, we have also visualised two translation sites that appear to fuse repeatedly then move apart (Movie 6, Fig. S5B). Whether this relates to random movement of translation sites or is associated with some regulation of translation will require further study. Together, these data show that the approaches we have described allow global translation dynamics to be elucidated, and different steps in the translation cycle to be visualised at single-mRNA resolution, in living embryos in real-time.

DISCUSSION

Here, we have applied the SunTag method to the *Drosophila* embryo, with fixed and live imaging, to study the translation of *hb* mRNAs at single-mRNA resolution during early embryogenesis. Our data from fixed embryos show uniform translation efficiency of *SunTag-hb* mRNAs across the expression domain during nc12 and nc13. We used the proximal *hb* enhancer to drive expression, which results in broadly uniform mRNA levels that decline towards the posterior border in nc12-14 (Bothma et al., 2015; Garcia et al., 2013). A similar shape of mRNA gradient is observed from the endogenous locus in nc12-13, when a shadow enhancer that activates expression in the same pattern to the proximal enhancer is also active (Bothma et al., 2015; Perry et al., 2011). Based on the profile we detect for the proportion of translated mRNAs, and the relatively constant ribosome number on mRNAs at nc13 irrespective of their position in the expression domain, our data predict that Hb protein levels decline between ∼30% and 50% EL at nc13 (Fig. 7A). This is entirely consistent with a quantitative measurement of Hb levels early in nc14 (Perry et al., 2012).

In nc14, we detect less *SunTag-hb* mRNA translation overall and the distribution of translation sites changes. Analysis of fixed embryos reveals that *SunTag-hb* mRNA translation is largely repressed in the anterior but persists in a band at the posterior border of the expression domain. Our live-imaging data provide a more complete picture of how the number and pattern of translation sites evolve over developmental time. There is an increase in the number of translation sites from nc11, with the highest number detected at mid-nc13. From late nc13, there is a gradual shift in the AP position of the peak of translation towards the posterior, culminating in

Development (2021) 148, dev196121. doi:10.1242/dev.196121

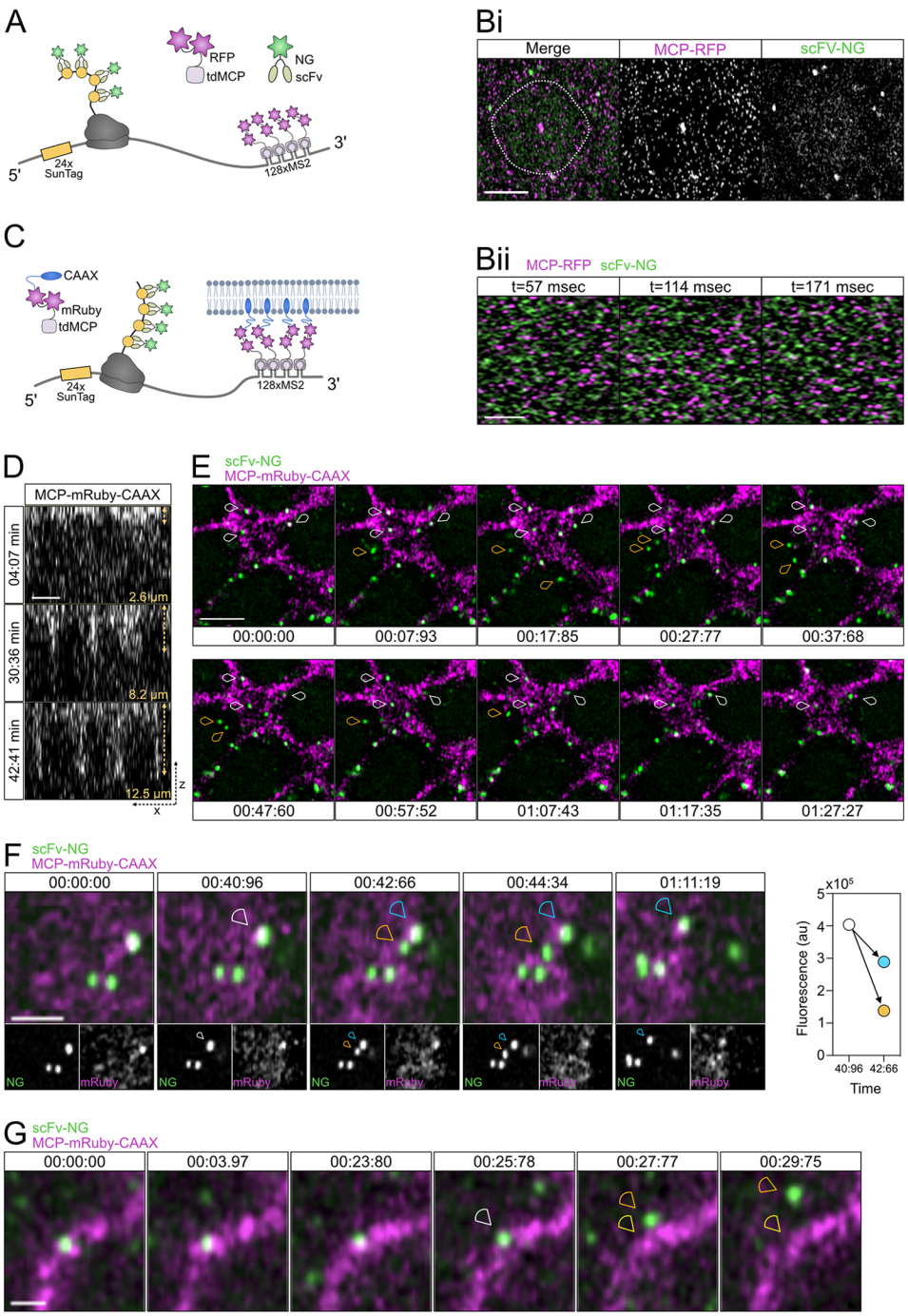

Fig. 6. Live imaging of *SunTag-hb-MS2* mRNAs detects different stages in the translation cycle. (A) Schematic outlining the live-imaging system used to visualise both *SunTag-hb-MS2* mRNA using MCP-RFP and translation sites using scFv-NG. (Bi) A still from a live-imaging movie showing that the tdMCP-RFP protein can be used to visualise the transcription site in the nucleus and single cytoplasmic mRNAs (magenta), in addition to visualisation of translation sites by scFv-NG proteins (green). The nuclear volume is outlined by the dashed white line based on the nuclear scFv-NG background. (Bii) Stills from Movie 2 showing tdMCP-RFP and scFv-NG signals in successive frames. (C) Schematic showing a modified live-imaging system where mRNAs are targeted to the cell membrane by the addition of a CAAX sequence to tdMCP-mRuby3. tdMCP-mRuby3-CAAX that is not bound to mRNA is also present in the membrane. (D) An orthogonal view of a *Drosophila* embryo during nc14 shows that tdMCP-mRuby3-CAAX is incorporated into the plasma membrane and cellularisation can be followed by the membrane ingression. (E) Translation sites (green) tethered at the plasma membrane through tdMCP-mRuby3-CAAX (magenta) can be followed for minutes (white arrowheads), whereas cytoplasmic proteins are visible more transiently (orange arrowheads). Time intervals are min:s:ms. See Movie 3. (F) Translation site dynamics are captured using the CAAX anchored system. A single protein (orange arrowhead, highly mobile) is detected leaving the translation site (white arrowhead), while more ribosomes continue translation of the same mRNA (blue arrowhead). Quantitation of the fluorescent signals suggests that the translation site in the plane of view contained ~four proteins being translated at time 00:40:96, of which three continue being translated at time 00:42:66. Time intervals are min:s:ms. See Movie 4.
(G) A translation site was followed (white arrowhead) until translation was terminated, resulting in a single protein leaving the translation site (orange arrowhead, highly mobile) with the mRNA still visible (yellow arrowhead). Time intervals are min:s:ms. See Movie 5. Scale bars: 5 µm in Bi, D and E; 2 µm in Bii, F; 1 µm in G.

SunTag-hb mRNA translation only being detected at the posterior of the expression domain in nc14 (Fig. 7A). *SunTag-hb* mRNAs are still present in the anterior in nc14, but ~95% are not being translated, suggesting that they are being translationally repressed.

In addition to the highest number of *SunTag-hb* mRNA translation sites being detected at nc13, analysis of the number of ribosomes translating the mRNAs in nc13 and 14 reveals that *SunTag-hb* mRNAs are more heavily translated in nc13. In nc14, the low number of mRNAs that are still being translated in the anterior are more poorly translated than those in the posterior, because we observe around half the number of ribosomes on anterior mRNAs compared with those at the posterior border. Currently, the mechanism underlying repression of *SunTag-hb* mRNAs in the anterior in nc14 is unknown. Given that the *hb* mRNA levels are high in the region where translation repression occurs, but low where translation persists, one obvious candidate would be negative feedback by the Hb protein itself, which would take longer to reach a threshold at the posterior of the expression domain. If Hb does negatively regulate translation of its mRNA, this regulation is likely indirect because Hb lacks an obvious RNA-binding domain.

The *hb* locus also has a stripe enhancer that activates transcription in a central and posterior stripe at nc14, with the central stripe positioned in the region where the early anterior expression domain ends (Margolis et al., 1995; Perry et al., 2012). As a result, the amount

Development (2021) 148, dev196121. doi:10.1242/dev.196121

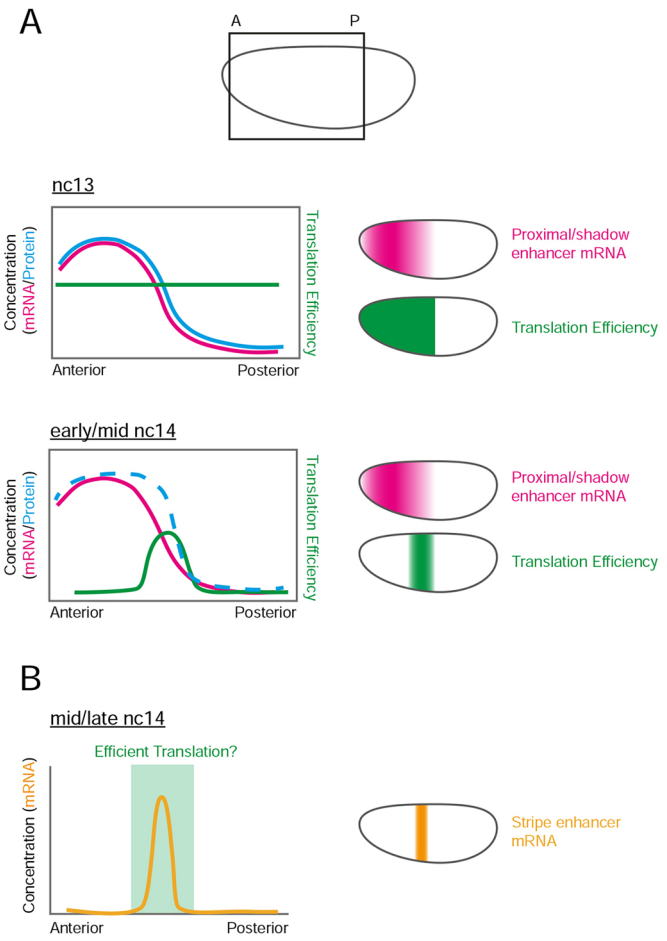

Fig. 7. Hypothesis for the interplay between transcriptional and translational regulation of *hb*. (A) Schematic of an embryo showing the area that the graphs in the figure represent. Graphs and embryos show the approximate output from the proximal enhancer. The shadow enhancer outputs a similar pattern. In nc13, translation efficiency (green) is constant and protein concentration (blue) reflects mRNA concentration (pink). In early/mid nc14, efficient translation is limited to the posterior edge of the mRNA expression domain, sharpening the protein concentration border (dashed blue line indicates a hypothetical output). (B) Hypothetical relationship to the stripe enhancer mRNA output. Stripe enhancer mRNA expression (yellow) occurs at the edge of the anterior expression domain. Efficient translation of this mRNA, in the area identified in A (nc14), would enhance the sharpness of the protein border.

of Hb protein is increased in this region (~40-50% EL) in nc14 embryos, which is necessary for Hb to specify the mesothoracic T2 segment by allowing activation of *Antennapedia* (Perry et al., 2012; Wu et al., 2001). Therefore, we suggest that the translational regulation that we have visualised using the simpler system of only the proximal enhancer will also exist for the more complex pattern of *hb* mRNAs transcribed under the control of the three *hb* enhancers in the endogenous locus. Such a mechanism of prolonged translation in the posterior of the expression domain would allow *hb* mRNAs that are transcribed due to activation from the stripe enhancer to be translated, promoting development of T2. Perhaps negative feedback downstream of Hb at the translational level functions together with the ability of Hb to repress its own transcription (Little et al., 2013; Perry et al., 2012) to establish a specific level and precise pattern of Hb, which are essential for correct AP patterning.

We propose that the increased translation efficiency of *SunTag-hb* mRNAs that we detect in the centre of the embryo at nc14, along with the extra transcription from the stripe enhancer, will complement each other in nc14 to reduce heterogeneity in Hb protein expression across the expression domain and sharpen its boundary (Fig. 7) (Perry et al., 2012; Wu et al., 2001). These mechanisms may also work together to filter positional errors in the Bcd gradient, with such a noise-filtering mechanism suggested for the generation of a precise Hb boundary (Houchmandzadeh et al., 2002; Yang et al., 2020). Earlier in development, in nc13, the proximal and shadow enhancers that activate transcription in the broad anterior domain function additively in the centre of the embryo, thereby maximising the transcriptional output where Bcd concentration is limiting, whereas the enhancers function subadditively more anteriorly (Bothma et al., 2015). Therefore, it appears that the embryo uses multiple mechanisms to shape the boundary of the anterior Hb expression domain during early embryogenesis. Future work studying the translation of *hb* mRNAs transcribed from the endogenous locus will allow fuller dissection of the interplay between transcriptional and translational regulation in generating the Hb protein profiles spatiotemporally.

We also show that translated mRNAs have a tendency to be in a slightly more open conformation compared with untranslated mRNAs, as described in mammalian cells (Adivarahan et al., 2018; Khong and Parker, 2018). The closed loop model for translation initiation proposes an association between the 5′ and 3′ ends of the mRNA, mediated by translation factors, to explain the synergistic effects of the cap and polyA tail on translation (Vicens et al., 2018). Our findings can still be compatible with this closed-loop model if, as suggested, the interaction between the 5′ and 3′ ends of the mRNA is relatively transient (Adivarahan et al., 2018; Archer et al., 2015; Khong and Parker, 2018) and/or the mRNA cycles between different conformations during the translation initiation steps (Costello et al., 2017). Alternatively, *hb* mRNA translation may be less reliant on the closed loop, with the requirement for the closed loop model for translation proposed to be mRNA dependent (Costello et al., 2015; Thompson et al., 2016). We also find no significant difference in mRNA compaction for untranslated mRNAs in the anterior and posterior in nc14 embryos, suggesting that the repression mechanism does not involve a major change in the degree of association of the 5′ and 3′ ends.

In live-imaging experiments using the scFv-NG fusion and standard MCP-fluorescent protein fusion, we found that the speed with which mRNAs move in 3D and the density of mRNAs in the cytoplasm preclude tracking of individual mRNAs over time. Two strategies have been used to overcome this same problem in mammalian cells, including tethering the mRNAs to the membrane (Yan et al., 2016) or studying local protein synthesis on the endoplasmic reticulum (Wu et al., 2016). By exploiting the membrane-tethering approach (Yan et al., 2016), we show that translation of individual mRNAs in the embryo can be monitored for at least 6 min, allowing events such as release of nascent proteins or translation termination to be captured.

The different MCP and scFv lines that we have generated will facilitate the quantitative study of translation of other *Drosophila* mRNAs, in live and/or fixed samples. Consistent with this, we note that another study, carried out in parallel to ours, also recently described the application of the SunTag approach to the study of *twi* mRNA translation in the *Drosophila* embryo (Dufourt et al., 2020 preprint). Overall, the quantitative data from the fixed SunTag embryo images and dynamic information about translation sites gained from imaging live embryos represent a powerful combination for probing the spatiotemporal regulation of translation. Future studies can also exploit the many advantages of the early embryo, such as the

Development (2021) 148, dev196121. doi:10.1242/dev.196121

synchronous nuclear divisions, which will allow the regulation of translation during mitosis to be studied without the need for drugs to arrest the cell cycle. Moreover, the SunTag approach can be used to reveal, at unparalleled spatiotemporal resolution, how the integration of transcription and translation dynamics shapes developmental patterning.

MATERIALS AND METHODS

Generation of plasmids and fly lines

phbP2>24xGCN4-hb-24xMS2, phbP2>24xGCN4-hb-128xMS2 and phbP2>24xGCN4-hb

The *hb* P2 enhancer, 5′UTR, coding sequence and 3′UTR were PCR amplified from genomic DNA. The SunTag (24×GCN4 peptides) was PCR amplified from the plasmid pcDNA4TO-24xGCN4_v4_sfGFP (Addgene #61058) (Tanenbaum et al., 2014), the 4xMS2 stem loop sequence was purified from pCR-24xMS2SL-stable (Addgene #31865) by restriction digest and the 128xMS2 from pMK123-128xMS2 (Tantale et al., 2016). The *hb* P2 enhancer, 5′UTR, 24xGCN4 and *hb* CDS were inserted into the StuI/BamHI sites of pUASP-attB (DGRC #1358) using multiple-insert In-Fusion cloning. The *hb* 3′UTR was inserted into the BamHI/NdeI sites. 24xMS2 and 128xMS2 were inserted into the BamHI site. The sequences of all primers used are shown in Table S1. φC31-based integration was used for specific integration of the transgenes into site 86Fb (chr3) by the University of Cambridge microinjection service.

pCasper-nos>tdMCP-2xRuby3-CAAX

tdMCP and mRuby3 were cloned into pCasper4 containing an attB site, the *tubulin* 3′UTR+1 kb downstream sequence in the XbaI site and the *nos* promoter in the EcoRI site. The NLS-HA-tdMCP from pHsp83-NLS-HA-2xMCP-2xTagRFP-T (Addgene #71242) (Halstead et al., 2016) was inserted into KpnI and SpeI-digested plasmid. 2xmRuby3 with a short linker was generated by introducing a second copy of mRuby3 into the BglII site of pKanCMV-mRuby3-10aa-H2B (Addgene #74258). The two copies of mRuby3 were then subcloned into the SpeI site of pCasper-nos>NLS-HA-tdMCP-tub3′UTR+1 kb. The CAAX from pHR-PP7-2xmCherry-CAAX (Addgene #74925) (Yan et al., 2016) was inserted between SpeI and BamHI. The NLS and HA tag were subsequently removed by digestion with Acc65I/NheI, the overhangs generated were filled using Klenow Fragment and the plasmid was religated. Transgenes were injected into w^{1118} flies using random P-element insertion. A line with the transgene located on the third chromosome was used for this study.

pCasper-nos>scFv-mNeonGreen-GB1-NLS and pCasper-nos>scFv-mNeonGreen-GB1

The scFv sequence was obtained from plasmid pHR-scFv-GCN4-sfGFP-GB1-NLS-dWPRE (Addgene #60906) (Tanenbaum et al., 2014). scFv-mNeonGreen-GB1-NLS was assembled using In-Fusion HD Cloning Plus multiple insert cloning (Takara Bio #638911) and integrated into the KpnI/SpeI sites of pCasper-attB-nos>tub3′UTR+1 kb (containing the *nos* promoter in EcoRI to direct maternal expression and *tubulin* 3′UTR+1 kb of downstream sequence in XbaI). To generate the noNLS version, the scFv-mNeonGreen-GB1 was amplified by PCR and inserted into KpnI/NotI of pCasper-attB-nos>tub3′UTR. φC31-based integration was used for specific re-integration of the transgene into sites 25C6 (chr2) and 86Fb (chr3) by the University of Cambridge microinjection service.

Fly stocks

Fly stocks used were: y^1w^{67c23} (used as wild type, BL6599), *P{w[+mC]=His2Av-mRFP1}III.1* (BL23650), *P{w+, pHsp83-NLS-HA-2xMCP-2xtagRFP}9/TM3* (Halstead et al., 2016). The following fly stocks were generated by insertion into 86Fb: *hbP2>24xGCN4-hb, hbP2>24xGCN4-hb-24xMS2, hbP2>24xGCN4-hb-128xMS2 and nos>scFv-mNeonGreen-GB1-NLS*. The following flies have insertions in 25C6: *nos>scFv-mNeonGreen-GB1-NLS* and *nos>scFv-mNeonGreen-GB1* (no NLS). The *nosP>tdMCP-2xmRuby3-CAAX* flies have a random insertion on the 3rd chromosome. The fixed embryos were collected from females homozygous for the *nos>scFv-mNeonGreen* transgene on the 2nd chromosome crossed to males homozygous for the *hb* reporter. To collect embryos from females with 3 or 4 copies of the *nos>scFv-mNeonGreen* transgene, the following fly stocks were made: *nos>scFv-mNeonGreen-GB1-NLS; nos>scFv-mNeonGreen-GB1-NLS/MKRS* and *nos>scFv-mNeonGreen-GB1-NLS; nos>scFv-mNeonGreen-GB1-NLS*. For the live imaging, males carrying the *hb* reporter were crossed to females of the following genotypes: *nos>scFv-mNeonGreen-GB1-NLS/+; HisRFP/+* (Fig. 5), *nos>scFv-mNeonGreen-GB1-NLS/CyO; pHsp83-NLS-HA-2xMCP-2xtagRFP/+* or *nos>scFv-mNeonGreen-GB1-NLS/+; nosP>tdMCP-2xmRuby3-CAAX/+* (Fig. 6). Flies were maintained at 18°C and crosses performed at 25°C. Flies were raised on standard fly food (yeast 50 g/l, glucose 78 g/l, maize flour 72 g/l, agar 8 g/l, nipagen 27 ml/l and propionic acid 3 ml/l). For smFISH/IF experiments, embryos were laid on apple juice agar plates with yeast paste for 1-4 h at 25°C prior to fixation.

Embryo fixation

Embryos were dechorionated for 2 min in 50% bleach and washed with water/Triton NaCl solution. They were then transferred to 1:3:4 37% formaldehyde: heptane: fixing solution [1.33× PBS, 0.07 M EGTA (pH 8.0)] and shaken for 20 min at 300 rpm. Embryos were devitellinised by the addition of methanol and shaking/vortexing.

smFISH/smiFISH and immunofluorescence

Fixed embryos were rocked at room temperature in glass scintillation vials in a series of washes: 5 min 50:50 methanol:PBT (1× phosphate buffered saline+0.1% Tween-20); 4×10 min PBT; 10 min 50:50 PBT:Stellaris wash buffer (10% formamide, 2× SSC); 2×5 min Stellaris wash buffer. Embryos were then allowed to settle for 5 min in Stellaris hybridisation buffer (100 mg/ml dextran sulphate, 10% formamide, 2× SSC). Stellaris hybridisation buffer was removed and replaced with fresh hybridisation buffer, and embryos were incubated in a 37°C water bath for 2 h as a prehybridisation step. Probe sets for smFISH (Biosearch Technologies) or smiFISH (Sigma Aldrich) were diluted in Stellaris hybridisation buffer to a final concentration of 100 nM (smFISH probes) and 80 nM (smiFISH probes) and embryos were incubated with probes in the dark at 37°C for at least 14 h. Following probe hybridisation, embryos were kept in the dark. Embryos were washed for 30 min, rinsed and washed for 3×15 min at 37°C, all with Stellaris hybridisation buffer prewarmed to 37°C. Embryos were then washed for 15 min at room temperature in Stellaris wash buffer, followed by washing for 3×10 min in PBT. Embryos were blocked for 30 min in PBT+1× Western Blocking Reagent (WBR, Sigma, 11921673001) and then incubated overnight at 4°C with primary antibody [mouse anti-mNeonGreen (32F6), Chromotek, 1:250] diluted in PBT+1× WBR. Embryos were rinsed twice in PBT, washed 4×15 min in PBT and blocked for 30 min in PBT+1× WBR. They were then incubated with secondary antibody (donkey anti-mouse Alexa Fluor 488 (A21202), Thermo Fisher Scientific, 1:250) diluted in PBT+1× WBR for 2 h at room temperature. Embryos were rinsed twice and washed 4×15 min in PBT, with the third wash including DAPI at 1:1000. They were then mounted on slides in ProLong Diamond Antifade Mountant (Thermo Fisher Scientific, 36961). smFISH/smiFISH probe sequences are shown in Table S1.

Static image acquisition

Images used for the analysis of mRNA and translated mRNA number were acquired using a Leica TCS SP8 AOBS inverted microscope using a 63×/1.40 oil objective and 0.75× confocal zoom. The confocal settings were pinhole 1 airy unit, scan speed 400 Hz unidirectional line scanning, 2× line averaging and a 2048×2048-pixel format. Images were collected sequentially with either Photon Multiplying Tube Detectors or Hybrid Detectors and illuminated using a white laser at 70%. The following detection mirror settings were used: Photon Multiplying Tube Detector DAPI excitation at 405 nm (2%, collection: 415-470 nm); Hybrid Detectors: AlexaFluor 488 excitation at 490 nm (10%, collection: 500-540 nm) and Quasar 570 excitation at 548 nm (15%, collection: 558-640 nm). Optical *z*-stacks were acquired at 300 nm spacing.

Images used for compaction analysis and quantitation of ribosome number were acquired with a Leica TCS SP8 AOBS inverted microscope

Development (2021) 148, dev196121. doi:10.1242/dev.196121

using a 100×/1.40 HC PL Apo CS2 oil objective and 3× confocal zoom. The confocal settings were as follows: pinhole 0.65 airy unit, scan speed 400 Hz bidirectional line scanning, 4× line averaging and a 4096×4096-pixel format. Images were collected sequentially with either Photon Multiplying Tube Detectors or Hybrid Detectors and illuminated using a white laser at 70%. The following detection mirror settings were used: Photon Multiplying Tube Detector DAPI excitation at 405 nm (11%, collection: 415-470 nm); Hybrid Detectors: AlexaFluor 488 excitation at 490 nm (12%, 1 to 6 µs gating, collection: 500-540 nm), Quasar 570 excitation at 548 nm (20%, 1 to 6 µs gating, collection: 558-640 nm) and Quasar 670 excitation at 647 nm (21%, 1 to 6 µs gating, collection: 668-779 nm). Optical *z*-stacks were acquired at 200 nm spacing.

Images of embryos with different numbers of maternal scFv- NG copies were acquired with a Leica TCS SP8 AOBS inverted microscope using a 40×/1.30 HC PL Apo CS2 oil objective and 1× confocal zoom. The confocal settings were as follows: pinhole 0.8 airy unit, scan speed 400 Hz bidirectional line scanning, 4× line accumulation and a 4752×4752-pixel format. Images were collected sequentially using the same laser and detector settings as described in the previous paragraph.

All raw images were deconvolved using Huygens Professional software (SVI) and figures show maximum intensity projections unless stated otherwise in the figure legends. All embryos are oriented with the anterior to the left. In the figure panels that focus on the anterior region of the embryo, the image is rotated and shown on a black background.

Live imaging microscopy

Embryos were dechorionated in bleach and mounted onto a Lumox imaging dish (Sarstedt, 94.6077.305) as described (Hoppe and Ashe, 2021). To visualise translation sites globally together with maternally deposited His-RFP, embryos were imaged using an LSM 880 microscope with an Airyscan Fast detector and an EC Plan-Neofluar 40×/1.30 oil DIC M27 objective at 1.1× optical zoom. In total, 25 planes were acquired with 850 nm spacing at 2996×788 pixels, with a *z*-stack acquisition time of ∼40 s. His-RFP was excited by the 561 nm laser line at 1.5% laser power and scFv-NG by the 488 nm laser line at 5%.

Live translation and the MCP-RFP-bound *SunTag-hb* mRNAs were imaged using an LSM 980 microscope with an Airyscan Fast detector to facilitate fast sampling times. Images were acquired using a PL Apo 63×/1.40 Oil objective at 8 bit, 17× optical zoom, with 2× line averaging and bidirectional scanning at an LSM scan speed of 9. MCP-RFP was excited by the 594 nm laser line at 7% laser power and scFv-NG by the 488 nm laser line at 2.2% laser power. A single plane time series was acquired at 176×160 pixels and with a frame time of ∼57 ms.

All other time-lapse data sets showing live translation were acquired on the LSM 880 with Airyscan Fast setup using a PL Apo 63×/1.40 Oil objective, unidirectional scanning at 16 bit and fluorophore excitation using the 594 nm laser line at 15% laser power and 488 nm laser line at 15% laser power. Additional specifications were as follows: MCP-RFP and scFV-NG: images showing nascent *hb* transcription were acquired at 8× optical zoom, 252×252 pixels, two optical slices 400 µm spaced apart and a time resolution of ∼842 ms per frame. A single plane is shown in in Fig. 6Bi. MCP-Ruby3-CAAX and scFV-NG: single plane time-lapse data sets were acquired at 8× optical zoom and with 184×184 pixels (overview and translation termination) and a time resolution of ∼2 s per frame or at 116×116 pixels (single protein release) with a time resolution of ∼1.7 s per frame. MCP-Ruby-CAAX orthogonal view: an embryo was imaged throughout nc14 at 0.7× optical zoom, 2176×1384 pixels. An optical stack was acquired with 1 µm spacing and a total depth of 16 µm, resulting in a final time resolution of ∼123 s.

Western blot

Drosophila embryonic extracts were prepared based on published protocols (Guilgur et al., 2014; Prudêncio and Guilgur, 2015). First, 1 to 4 h-old embryos were dechorionated and homogenised in ice cold lysis buffer [150 mM NaCl, 20 mM Tris.HCl (pH 8), 2 mM EDTA, 0.1% NP-40, 1 mM DTT, 1× cOmplete, EDTA-free Protease Inhibitor Cocktail (Sigma 11873580001)]. Extracts were centrifuged at 15,000 ***g*** for 20 min at 4°C. Lysates were denatured in NuPAGE LDS Sample Buffer (4×) (Thermo Fisher Scientific, NP0007) with 50 mM DTT. A standard western blot protocol was used with anti-HA(12CA5) (1:1000, Merck 11583816001), anti-Actin(20-33) (1:1000, Merck A5060) and anti-mNeonGreen (1:1000; Chromotek, 32F6), and IRDye 680RD donkey anti-rabbit IgG (H+L) (1:10,000, Li-Cor 926-68073) and IRDye 800CW donkey anti-mouse IgG (H+L) (1:10,000, Li-Cor 926-32212). Signals were detected using the Li-Cor Odyssey CLx Infrared detection system.

Quantitation of the number of total and translated mRNAs

For analysis of mRNA and translation site number, fixed embryos were stained with SunTag smFISH probes, anti-mNeonGreen antibody and DAPI, and imaged using the acquisition details described above. *SunTag* mRNAs and mNeonGreen foci were identified using the Imaris software (Imaris software 9.2; Bitplane, Oxford Instruments) 'spots' function. *SunTag* mRNA puncta were identified with spot volume 0.6 µm in diameter and 1.2 µm in the *z* direction. mNeonGreen foci were identified with spot volume 0.5 µm in diameter and 1 µm in the *z* direction. Nuclei were identified using the Imaris 'surfaces' function. Translated mRNAs were identified using the Imaris 'Co-localise Spots' Xtension, with mRNA and NG spots called as colocalised if the distance between the centroids of the two spots was less than 0.6 µm. Spots inside the nucleus were identified using the Imaris 'Split Into Surface Objects' Xtension. Nuclear spots were excluded by combining the data for all spots and removing any duplicated spots. Spot IDs were then used to extract statistics for cytoplasmic spots, which were used for analysis.

Cytoplasmic spots were assigned to surfaces using a modified version of spotMe.py from (Hoppe et al., 2020), spotMe_EmbryoMid.py. Spot assignment to surfaces remains unchanged, while midline detection is modified to fit the midline of the embryo rather than the expression domain. Given that only a part of the embryo is obtained in each frame, and the orientation of the embryo can vary, the midline is detected by identifying the edge nuclei of the embryo. Nuclei within 1.5 internuclear distances of the edge of the frame are removed. Centroids for all permutations of unique nuclei pairs from opposing edges of the embryo are calculated creating a coordinate set representing the mean position between the two embryo edges. These mean positions are used to calculate the midline using a least-squares approach. The anterior position of the embryo is determined by identifying the end of the embryo with the least nuclei in bins along the *x*-axis. Positions along the AP axis of the embryo for each nucleus are determined by assigning nuclei to their closest position on the AP axis then calculating the distance between that AP position and the position closest to the anterior-most nuclei. The code used can be found at https://github.com/TMinchington/sass. In nc14 embryos with either the *SunTag-hb* or *SunTag-hb-MS2* transgenes, we observed 25/26 embryos with a band of translation sites and 1/26 embryo with uniform translation sites. Given that we only found a single nc14 embryo with uniform translation sites, we consider that it had a developmental defect. Three embryos with a band were fully analysed.

Compaction and ribosome number

For compaction and ribosome number analysis, fixed *Drosophila* embryos were stained with smFISH probes against the *SunTag*-coding sequence, smiFISH probes against the *hb*-coding sequence, and anti-mNeonGreen antibody. The two probe sets, targeting different regions of the *hb* transgene, are spaced 3092 nucleotides between their centres. Anterior and posterior regions were imaged with a 100× objective and 3× optical zoom (acquisition details described above). Regions of these images were analysed for compaction and ribosome number quantitation.

For compaction analysis, *SunTag* (5′ probe) and *hb* (3′ probe) mRNA foci as well as mNeonGreen translation sites were identified using the Imaris 'spots' function (Imaris software 9.2) and their statistics exported. The closest distance in three dimensions between a *SunTag* spot and its corresponding *hb* spot was computed based on the spot centroids using a custom python script. Foci were assumed to be from the same mRNA if they were less than 300 nm apart. mRNAs were classified as translating if the distance between a *SunTag* spot centroid and the nearest mNeonGreen centroid was less than 300 nm.

Development (2021) 148, dev196121. doi:10.1242/dev.196121

For ribosome number analysis, the fluorescence intensity of *SunTag* mRNA and mNeonGreen signal was quantitated using the AirLocalize software to quantitate the number of ribosomes within a translation site (Trcek et al., 2017). AirLocalize outputs were used to perform a colocalisation analysis using custom python scripts to classify the mNeonGreen signal into translation sites and single proteins. The number of ribosomes present in translation sites, which were assigned based on colocalisation with a mRNA, was calculated using the median fluorescence intensity of single proteins and corrected for the position of the GCN4 repeats. A correction factor was used, calculated by $(length_{SunTagCDS}\times0.5+length_{hbCDS})/length_{total}$, to account for ribosomes that had only translated a fraction of the SunTag repeat (Pichon et al., 2016). Ribosome numbers larger than five could be confidently identified and are presented in Fig. 4Di-ii.

Nuclear scFv-NG concentration

Nuclear scFv-NG levels were quantitated from static images of *Drosophila* embryos whose mothers carried 2×, 3× or 4× copies of scFv-NG. Nuclei positioned outside of the *hb* expression domain, in the posterior region of the embryo, were segmented using the 'surface' function in Imaris. The sum fluorescence intensity of a nucleus in the scFv-NG channel was divided by the nuclear area. Background levels were estimated using 'spot' objects placed in the cytoplasm between posterior nuclei. The sum fluorescent background value was divided by the spot area and subtracted from the nuclear fluorescence.

Nuclear tracking and translation site identification in live-imaging datasets

Nuclei were segmented and tracked in the Imaris software based on the His-RFP fluorescent signal. Nuclei were segmented using the 'surface function' individually for each nuclear cycle and then tracked through time using the inbuilt autoregressive motion tracking with a maximum frame gap size of 5 frames and a maximum travel distance of 6 µm. The scFv-NG channel was first smoothed and blurred using a wavelet filter (Imaris X-tension; Hoppe and Ashe, 2021) and translation sites were then identified using the Imaris 'spots' function. Translation sites were estimated to have *xy* diameter 0.7 µm with a *z*-axis point spread function estimation of 1.4 µm. To determine the background fluorescence in the translation site channel, a set of 'spots' of the same volume was generated for background correction. Statistics were exported for tracked surfaces, translation site spots and background spots. Translation sites were linked to their closest nucleus (nuclear territories) and background correction was applied using the custom python script 'sass' (https://github.com/TMinchington/sass) (Hoppe et al., 2020).

Translation site fluorescence and tracks

Fluorescent translation sites were quantitated using the Imaris 'spots' function and sum fluorescence values are reported in Fig. 6F. Spot sizes were chosen to contain the full translation site fluorescence. Background fluorescence was determined using spots of the same size as translation spots and the sum fluorescence was subtracted from translation sites. To track translation site fluorescence through time, the Imaris inbuilt spot tracking function was used. Individual fluorescent traces of translation sites through time are shown in Fig. S5.

Statistical analysis

Statistical comparisons were performed using one-way ANOVA or Kruskal–Wallis tests with multiple comparison, two-tailed Student's *t*-test or paired Student's *t*-test using GraphPad Prism and R (Version 3.5.2). The statistical test used and the respective sample size can be found in the figure legends. Statistical significance was assumed at $P<0.05$ and individual *P* values are indicated in the figure legends.

Acknowledgements

We thank Mark Ashe for helpful discussions, Nathan Garnham for help generating the transgenes, Edouard Bertrand for the pMK123-128xMS2 plasmid, Frank Wippich and Anne Ephrussi for the MCP-RFP flies, Shane Herbert for microscopy time, and the University of Manchester Bioimaging Facility for support.

Competing interests

The authors declare no competing or financial interests.

Author contributions

Conceptualisation: D.J.V., H.L.A.; Software: T.G.M.; Investigation: D.J.V., C.H., C.S.; Writing - original draft: D.J.V., H.L.A.; Writing - review & editing: D.J.V., C.H., H.L.A.; Supervision: H.L.A.; Funding acquisition: H.L.A.

Funding

This work was funded by a Wellcome Trust Investigator Award to H.L.A. (204832/Z/16/Z) and by a Wellcome Trust PhD studentship to D.V. (215206/Z/19/Z). Deposited in PMC for immediate release.

Peer review history

The peer review history is available online at https://journals.biologists.com/dev/article-lookup/doi/10.1242/dev.196121

References

Adivarahan, S., Livingston, N., Nicholson, B., Rahman, S., Wu, B., Rissland, O. S. and Zenklusen, D. (2018). Spatial organization of single mRNPs at different stages of the gene expression pathway. *Mol. Cell* **72**, 727-738.e725. doi:10.1016/j.molcel.2018.10.010

Archer, S. K., Shirokikh, N. E., Hallwirth, C. V., Beilharz, T. H. and Preiss, T. (2015). Probing the closed-loop model of mRNA translation in living cells. *RNA Biol.* **12**, 248-254. doi:10.1080/15476286.2015.1017242

Bender, M., Horikami, S., Cribbs, D. and Kaufman, T. C. (1988). Identification and expression of the gap segmentation genehunchback indrosophila melanogaster. *Dev. Genet.* **9**, 715-732. doi:10.1002/dvg.1020090604

Bothma, J. P., Garcia, H. G., Ng, S., Perry, M. W., Gregor, T. and Levine, M. (2015). Enhancer additivity and non-additivity are determined by enhancer strength in the Drosophila embryo. *eLife* **4**, e07956. doi:10.7554/eLife.07956.013

Cho, P. F., Gamberi, C., Cho-Park, Y. A., Cho-Park, I. B., Lasko, P. and Sonenberg, N. (2006). Cap-dependent translational inhibition establishes two opposing morphogen gradients in Drosophila embryos. *Curr. Biol.* **16**, 2035-2041. doi:10.1016/j.cub.2006.08.093

Costello, J., Castelli, L. M., Rowe, W., Kershaw, C. J., Talavera, D., Mohammad-Qureshi, S. S., Sims, P. F. G., Grant, C. M., Pavitt, G. D., Hubbard, S. J. et al. (2015). Global mRNA selection mechanisms for translation initiation. *Genome Biol.* **16**, 10. doi:10.1186/s13059-014-0559-z

Costello, J. L., Kershaw, C. J., Castelli, L. M., Talavera, D., Rowe, W., Sims, P. F. G., Ashe, M. P., Grant, C. M., Hubbard, S. J. and Pavitt, G. D. (2017). Dynamic changes in eIF4F-mRNA interactions revealed by global analyses of environmental stress responses. *Genome Biol.* **18**, 201. doi:10.1186/s13059-017-1338-4

Driever, W. and Nüsslein-Volhard, C. (1989). The bicoid protein is a positive regulator of hunchback transcription in the early Drosophila embryo. *Nature* **337**, 138-143. doi:10.1038/337138a0

Dufourt, J., Bellec, M., Trullo, A., Dejean, M., De Rossi, S. and Lagha, M. (2020). Imaging translation dynamics in live embryos reveals spatial heterogeneities. *bioRXiv*. doi:10.1101/2020.04.08.058974

Dunn, J. G., Foo, C. K., Belletier, N. G., Gavis, E. R. and Weissman, J. S. (2013). Ribosome profiling reveals pervasive and regulated stop codon readthrough in Drosophila melanogaster. *eLife* **2**, e01179. doi:10.7554/eLife.01179.026

Eichhorn, S. W., Subtelny, A. O., Kronja, I., Kwasnieski, J. C., Orr-Weaver, T. L. and Bartel, D. P. (2016). mRNA poly(A)-tail changes specified by deadenylation broadly reshape translation in Drosophila oocytes and early embryos. *eLife* **5**, e16955. doi:10.7554/eLife.16955.026

Garcia, H. G., Tikhonov, M., Lin, A. and Gregor, T. (2013). Quantitative imaging of transcription in living Drosophila embryos links polymerase activity to patterning. *Curr. Biol.* **23**, 2140-2145. doi:10.1016/j.cub.2013.08.054

Guilgur, L. G., Prudencio, P., Sobral, D., Liszekova, D., Rosa, A. and Martinho, R. G. (2014). Requirement for highly efficient pre-mRNA splicing during Drosophila early embryonic development. *eLife* **3**, e02181. doi:10.7554/eLife.02181

Halstead, J. M., Wilbertz, J. H., Wippich, F., Lionnet, T., Ephrussi, A. and Chao, J. A. (2016). TRICK: a single-molecule method for imaging the first round of translation in living cells and animals. *Methods Enzymol.* **572**, 123-157. doi:10.1016/bs.mie.2016.02.027

Hoppe, C. and Ashe, H. L. (2021) Live imaging and quantitation of nascent transcription using the MS2/MCP system in the Drosophila embryo. *STAR Protocols* **2**, 100379. doi:10.1016/j.xpro.2021.100379.

Hoppe, C., Bowles, J. R., Minchington, T. G., Sutcliffe, C., Upadhyai, P., Rattray, M. and Ashe, H. L. (2020). Modulation of the promoter activation rate dictates the transcriptional response to graded BMP signaling levels in the Drosophila embryo. *Dev. Cell* **54**, 727-741.e727. doi:10.1016/j.devcel.2020.07.007

Houchmandzadeh, B., Wieschaus, E. and Leibler, S. (2002). Establishment of developmental precision and proportions in the early Drosophila embryo. *Nature* **415**, 798-802. doi:10.1038/415798a

Hülskamp, M., Schröder, C., Pfeifle, C., Jäckle, H. and Tautz, D. (1989). Posterior segmentation of the Drosophila embryo in the absence of a maternal posterior organizer gene. *Nature* **338**, 629-632. doi:10.1038/338629a0

Hulskamp, M., Pfeifle, C. and Tautz, D. (1990). A morphogenetic gradient of hunchback protein organizes the expression of the gap genes Kruppel and knirps in the early Drosophila embryo. *Nature* **346**, 577-580. doi:10.1038/346577a0

Irish, V., Lehmann, R. and Akam, M. (1989). The Drosophila posterior-group gene nanos functions by repressing hunchback activity. *Nature* **338**, 646-648. doi:10.1038/338646a0

Khong, A. and Parker, R. (2018). mRNP architecture in translating and stress conditions reveals an ordered pathway of mRNP compaction. *J. Cell Biol.* **217**, 4124-4140. doi:10.1083/jcb.201806183

Lasko, P. (2012). mRNA localization and translational control in Drosophila oogenesis. *Cold Spring Harb. Perspect Biol.* **4**, a012294. doi:10.1101/cshperspect.a012294

Lehmann, R. and Nusslein-Volhard, C. (1987). hunchback, a gene required for segmentation of an anterior and posterior region of the Drosophila embryo. *Dev. Biol.* **119**, 402-417. doi:10.1016/0012-1606(87)90045-5

Little, S. C., Tikhonov, M. and Gregor, T. (2013). Precise developmental gene expression arises from globally stochastic transcriptional activity. *Cell* **154**, 789-800. doi:10.1016/j.cell.2013.07.025

Lucas, T., Ferraro, T., Roelens, B., De Las Heras Chanes, J., Walczak, A. M., Coppey, M. and Dostatni, N. (2013). Live imaging of bicoid-dependent transcription in Drosophila embryos. *Curr. Biol.* **23**, 2135-2139. doi:10.1016/j.cub.2013.08.053

Margolis, J. S., Borowsky, M. L., Steingrímsson, E., Shim, C. W., Lengyel, J. A. and Posakony, J. W. (1995). Posterior stripe expression of hunchback is driven from two promoters by a common enhancer element. *Development* **121**, 3067-3077.

Morisaki, T. and Stasevich, T. J. (2018). Quantifying single mRNA translation kinetics in living cells. *Cold Spring Harb. Perspect Biol.* **10**, a032078. doi:10.1101/cshperspect.a032078

Murata, Y. and Wharton, R. P. (1995). Binding of pumilio to maternal hunchback mRNA is required for posterior patterning in Drosophila embryos. *Cell* **80**, 747-756. doi:10.1016/0092-8674(95)90353-4

Perry, M. W., Boettiger, A. N. and Levine, M. (2011). Multiple enhancers ensure precision of gap gene-expression patterns in the Drosophila embryo. *Proc. Natl. Acad. Sci. USA* **108**, 13570-13575. doi:10.1073/pnas.1109873108

Perry, M. W., Bothma, J. P., Luu, R. D. and Levine, M. (2012). Precision of hunchback expression in the Drosophila embryo. *Curr. Biol.* **22**, 2247-2252. doi:10.1016/j.cub.2012.09.051

Pichon, X., Bastide, A., Safieddine, A., Chouaib, R., Samacoits, A., Basyuk, E., Peter, M., Mueller, F. and Bertrand, E. (2016). Visualization of single endogenous polysomes reveals the dynamics of translation in live human cells. *J. Cell Biol.* **214**, 769-781. doi:10.1083/jcb.201605024

Prudêncio, P. and Guilgur, L. G. (2015). Protein extraction from Drosophila embryos and ovaries. *Bio-protocol* **5**, e1459. doi:10.21769/BioProtoc.1459

Schröder, C., Tautz, D., Seifert, E. and Jäckle, H. (1988). Differential regulation of the two transcripts from the Drosophila gap segmentation gene hunchback. *EMBO J.* **7**, 2881-2887. doi:10.1002/j.1460-2075.1988.tb03145.x

Sonoda, J. and Wharton, R. P. (1999). Recruitment of Nanos to hunchback mRNA by Pumilio. *Genes Dev.* **13**, 2704-2712. doi:10.1101/gad.13.20.2704

Sonoda, J. and Wharton, R. P. (2001). Drosophila brain tumor is a translational repressor. *Genes Dev.* **15**, 762-773. doi:10.1101/gad.870801

Struhl, G. (1989). Differing strategies for organizing anterior and posterior body pattern in Drosophila embryos. *Nature* **338**, 741-744. doi:10.1038/338741a0

Struhl, G., Johnston, P. and Lawrence, P. A. (1992). Control of Drosophila body pattern by the hunchback morphogen gradient. *Cell* **69**, 237-249. doi:10.1016/0092-8674(92)90405-2

Struhl, G., Struhl, K. and Macdonald, P. M. (1989). The gradient morphogen bicoid is a concentration-dependent transcriptional activator. *Cell* **57**, 1259-1273. doi:10.1016/0092-8674(89)90062-7

Tanenbaum, M. E., Gilbert, L. A., Qi, L. S., Weissman, J. S. and Vale, R. D. (2014). A protein-tagging system for signal amplification in gene expression and fluorescence imaging. *Cell* **159**, 635-646. doi:10.1016/j.cell.2014.09.039

Tantale, K., Mueller, F., Kozulic-Pirher, A., Lesne, A., Victor, J. M., Robert, M. C., Capozi, S., Chouaib, R., Backer, V., Mateos-Langerak, J. et al. (2016). A single-molecule view of transcription reveals convoys of RNA polymerases and multi-scale bursting. *Nat. Commun.* **7**, 12248. doi:10.1038/ncomms12248

Tautz, D. and Pfeifle, C. (1989). A non-radioactive in situ hybridization method for the localization of specific RNAs in Drosophila embryos reveals translational control of the segmentation gene hunchback. *Chromosoma* **98**, 81-85. doi:10.1007/BF00291041

Tautz, D., Lehmann, R., Schnürch, H., Schuh, R., Seifert, E., Kienlin, A., Jones, K. and Jäckle, H. (1987). Finger protein of novel structure encoded by hunchback, a second member of the gap class of Drosophila segmentation genes. *Nature* **327**, 383-389. doi:10.1038/327383a0

Thompson, M. K., Rojas-Duran, M. F., Gangaramani, P. and Gilbert, W. V. (2016). The ribosomal protein Asc1/RACK1 is required for efficient translation of short mRNAs. *eLife* **5**, e11154. doi:10.7554/eLife.11154.033

Trcek, T., Lionnet, T., Shroff, H. and Lehmann, R. (2017). mRNA quantification using single-molecule FISH in Drosophila embryos. *Nat. Protoc.* **12**, 1326-1348. doi:10.1038/nprot.2017.030

Vicens, Q., Kieft, J. S. and Rissland, O. S. (2018). Revisiting the closed-loop model and the nature of mRNA 5′-3′ communication. *Mol. Cell* **72**, 805-812. doi:10.1016/j.molcel.2018.10.047

Voigt, F., Zhang, H., Cui, X. A., Triebold, D., Liu, A. X., Eglinger, J., Lee, E. S., Chao, J. A. and Palazzo, A. F. (2017). Single-molecule quantification of translation-dependent association of mRNAs with the endoplasmic reticulum. *Cell Rep.* **21**, 3740-3753. doi:10.1016/j.celrep.2017.12.008

Wang, C., Han, B., Zhou, R. and Zhuang, X. (2016). Real-time imaging of translation on single mRNA transcripts in live cells. *Cell* **165**, 990-1001. doi:10.1016/j.cell.2016.04.040

Wharton, R. P. and Struhl, G. (1991). RNA regulatory elements mediate control of Drosophila body pattern by the posterior morphogen nanos. *Cell* **67**, 955-967. doi:10.1016/0092-8674(91)90368-9

Wu, X., Vasisht, V., Kosman, D., Reinitz, J. and Small, S. (2001). Thoracic patterning by the Drosophila gap gene hunchback. *Dev. Biol.* **237**, 79-92. doi:10.1006/dbio.2001.0355

Wu, B., Chao, J. A. and Singer, R. H. (2012). Fluorescence fluctuation spectroscopy enables quantitative imaging of single mRNAs in living cells. *Biophys. J.* **102**, 2936-2944. doi:10.1016/j.bpj.2012.05.017

Wu, B., Eliscovich, C., Yoon, Y. J. and Singer, R. H. (2016). Translation dynamics of single mRNAs in live cells and neurons. *Science* **352**, 1430-1435. doi:10.1126/science.aaf1084

Yan, X., Hoek, T. A., Vale, R. D. and Tanenbaum, M. E. (2016). Dynamics of translation of single mRNA molecules In Vivo. *Cell* **165**, 976-989. doi:10.1016/j.cell.2016.04.034

Yang, Z., Zhu, H., Kong, K., Wu, X., Chen, J., Li, P., Jiang, J., Zhao, J., Cui, B. and Liu, F. (2020). The dynamic transmission of positional information in stau(-) mutants during Drosophila embryogenesis. *eLife* **9**, e54276. doi:10.7554/eLife.54276.sa2